

PNAS



1

2 **Supporting Information for**

3 **Joint models reveal human subcortical underpinnings of choice and learning behavior**

4 **Steven Miletić, Niek Stevenson, Pierre-Louis Bazin, Anneke Alkemade, Scott J. S. Isherwood, Anne C. Trutti, Desmond H. Y.**
5 **Tse, Asta K. Háberg, Birte U. Forstmann**

6 **Steven Miletić.**

7 **E-mail: s.miletic@fsw.leidenuniv.nl**

8 **This PDF file includes:**

- 9 Figs. S1 to S5
- 10 Tables S1 to S4
- 11 SI References

12 Supporting Methods

13 **Anatomical data preprocessing.** A total of 2 T1-weighted (T1w) images were found within the input BIDS dataset: One at
14 0.75 mm resolution from the anatomical session, and one at 1.0 mm resolution from the session including the task paradigm.
15 Both were corrected for intensity non-uniformity (INU) with `N4BiasFieldCorrection` (1), distributed with ANTs 2.3.3 (2,
16 RRID:SCR_004757). The T1w-reference was then skull-stripped with a *Nipype* implementation of the `antsBrainExtraction.sh`
17 workflow (from ANTs), using OASIS30ANTs as target template. Brain tissue segmentation of cerebrospinal fluid (CSF), white-
18 matter (WM) and gray-matter (GM) was performed on the brain-extracted T1w using `fast` (FSL 5.0.9, RRID:SCR_002823,
19 3). A T1w-reference map was computed after registration of 2 T1w images (after INU-correction) using `mri_robust_template`
20 (FreeSurfer 6.0.1, 4). Brain surfaces were reconstructed using `recon-all` (FreeSurfer 6.0.1, RRID:SCR_001847, 5), and the brain
21 mask estimated previously was refined with a custom variation of the method to reconcile ANTs-derived and FreeSurfer-derived
22 segmentations of the cortical gray-matter of Mindboggle (RRID:SCR_002438, 6). Volume-based spatial normalization to
23 one standard space (MNI152NLin2009cAsym) was performed through nonlinear registration with `antsRegistration` (ANTs
24 2.3.3), using brain-extracted versions of both T1w reference and the T1w template. The following template was selected for
25 spatial normalization: *ICBM 152 Nonlinear Asymmetrical template version 2009c*[(7), RRID:SCR_008796; TemplateFlow ID:
26 MNI152NLin2009cAsym].

27 **Functional data preprocessing.** For each of the 3 BOLD runs found per subject, the following preprocessing was performed.
28 First, a reference volume and its skull-stripped version were generated by aligning and averaging 1 single-band references
29 (SBRefs). A B0-nonuniformity map (or *fieldmap*) was estimated based on two EPI references with opposing phase-encoding
30 directions, with `3dQwarp` (8) (AFNI 20160207). Based on the estimated susceptibility distortion, a corrected EPI reference
31 was calculated for a more accurate co-registration with the anatomical reference. The BOLD reference was then co-registered
32 to the T1w reference using `bbregister` (FreeSurfer) which implements boundary-based registration (9). Co-registration was
33 configured with six degrees of freedom. Head-motion parameters with respect to the BOLD reference (transformation matrices,
34 and six corresponding rotation and translation parameters) are estimated before any spatiotemporal filtering using `mcflirt`
35 (FSL 5.0.9, 10). BOLD runs were slice-time corrected using `3dTshift` from AFNI 20160207 (8, RRID:SCR_005927). First, a
36 reference volume and its skull-stripped version were generated using a custom methodology of *fMRIPrep*. The BOLD time-series
37 (including slice-timing correction when applied) were resampled onto their original, native space by applying a single, composite
38 transform to correct for head-motion and susceptibility distortions. These resampled BOLD time-series will be referred to as
39 *preprocessed BOLD in original space*, or just *preprocessed BOLD*. Several confounding time-series were calculated based on
40 the *preprocessed BOLD*: framewise displacement (FD), ‘DVARs’ (the spatial standard deviation of difference images), and
41 three region-wise global signals. FD was computed using two formulations following Power (absolute sum of relative motions,
42 (11)) and Jenkinson (relative root mean square displacement between affines, (10)). FD and DVARs are calculated for each
43 functional run, both using their implementations in *Nipype* (following the definitions by 11). The three global signals are
44 extracted within the CSF, the WM, and the whole-brain masks. Additionally, a set of physiological regressors were extracted
45 to allow for component-based noise correction (*CompCor*, 12). Principal components are estimated after high-pass filtering
46 the *preprocessed BOLD* time-series (using a discrete cosine filter with 128s cut-off) for the two *CompCor* variants: temporal
47 (tCompCor) and anatomical (aCompCor). tCompCor components are then calculated from the top 2% variable voxels within
48 the brain mask. For aCompCor, three probabilistic masks (CSF, WM and combined CSF+WM) are generated in anatomical
49 space. The implementation differs from that of Behzadi et al. in that instead of eroding the masks by 2 pixels on BOLD space,
50 the aCompCor masks subtract a mask of pixels that likely contain a volume fraction of GM. This mask is obtained by dilating
51 a GM mask extracted from the FreeSurfer’s *aseg* segmentation, and it ensures components are not extracted from voxels
52 containing a minimal fraction of GM. Finally, these masks are resampled into BOLD space and binarised by thresholding at
53 0.99 (as in the original implementation). Components are also calculated separately within the WM and CSF masks. For each
54 CompCor decomposition, the k components with the largest singular values are retained, such that the retained components’
55 time series are sufficient to explain 50 percent of variance across the nuisance mask (CSF, WM, combined, or temporal). The
56 remaining components are dropped from consideration. The head-motion estimates, calculated in the correction step, were
57 also placed within the corresponding confounds file. The confound time series derived from head motion estimates and global
58 signals were expanded with the inclusion of temporal derivatives and quadratic terms for each (13). Frames that exceeded a
59 threshold of 0.5 mm FD or 1.5 standardised DVARs were annotated as motion outliers. All resamplings can be performed with
60 a *single interpolation step* by composing all the pertinent transformations (i.e. head-motion transform matrices, susceptibility
61 distortion correction when available, and co-registrations to anatomical and output spaces). Gridded (volumetric) resamplings
62 were performed using `antsApplyTransforms` (ANTs), configured with Lanczos interpolation to minimise the smoothing effects
63 of other kernels (14). Non-gridded (surface) resamplings were performed using `mri_vol2surf` (FreeSurfer).

64 Many internal operations of *fMRIPrep* use *Nilearn* 0.6.2 (15, RRID:SCR_001362), mostly within the functional processing
65 workflow. For more details of the pipeline, see [the section corresponding to workflows in *fMRIPrep*’s documentation](#).

66 **GLM specification.** In the main text, the GLM specifying the model of the neural timeseries as a function of the design matrix
67 omits the temporal derivatives, to improve readability. The full GLM includes the derivatives as follows:

$$\begin{aligned}
y = & \beta_0 + \\
& \beta_{trial} x_{cue} + \beta'_{trial} x'_{cue} + \\
& \beta_{spd-acc} x_{cue, spd-acc} + \beta'_{spd-acc} x'_{cue, spd-acc} + \\
& \beta_{trial} x_{response} + \beta'_{trial} x'_{response} + \\
& \beta_{left-right} x_{left-right} + \beta'_{left-right} x'_{left-right} + \\
& \beta_{trial} x_{stimulus} + \beta'_{trial} x'_{stimulus} + \\
& \beta_{\Delta value} x_{\Delta value} + \beta'_{\Delta value} x'_{\Delta value} + \\
& \beta_{trial} x_{feedback} + \beta'_{trial} x'_{feedback} + \\
& \beta_{RPE} x_{RPE} + \beta'_{RPE} x'_{RPE} + e \\
& e \sim \mathcal{N}(0, \sigma)
\end{aligned} \tag{1}$$

where each x refers to a regressor convolved with the canonical double-gamma haemodynamic response function, and x' to the regressors convolved with the temporal derivative of the canonical haemodynamic response function. β and β' refer to the corresponding parameters.

Deconvolution of heart rate variability and respiratory volume per time. We tested whether we could find different effects of the SPD and ACC cues on the physiological measures of heart rate variability (HRV) and respiratory volume per time (RVT), as potential proxies of arousal. We first obtained HRV and RVT through running PhysIO (detailed in the main text). Next, we applied a deconvolution approach. Specifically, we performed a deconvolution using Fourier basis sets (16, 17) with 7 regressors (an intercept, three sines, and three cosines) for two events of interest: The SPD and the ACC cues. Additionally, we added regressors for the effect of the stimulus presentation. The deconvolution models were fit with ordinary least squares, and implemented in Python package nideconv (18).

Supporting Results

Sensitivity analysis. To test whether our sample size, trial numbers, and fitting methods were sufficiently powerful to detect potential differences between learning rates in SPD and ACC trials, we performed a simulation study. In this study, we generated synthetic data in which we systematically varied the data-generating between-condition differences in learning rates $\Delta\alpha = \alpha_{ACC} - \alpha_{SPD}$. For each of ten datasets, we randomly sampled $\Delta\alpha_i$ for each participant i from $N(\Delta\alpha, 0.01)$. $\alpha_{SPD,i}$ was randomly sampled from $N(0.05, 0.01)$ for all datasets. For all other data-generating parameters, we used the subjectwise posterior median of the fit RL-ARD with two learning rates. This way, we ensured that our synthetic data respects the design properties of our dataset (the same number of participants, trials per participants, stimulus sets, and blocks), as well as the interindividual variability in decision parameters.

Then, we fit both the RL-ARD with a single α (RL-ARD1) and the RL-ARD with two learning rates ($\alpha_{ACC}, \alpha_{SPD}$; RL-ARD2) to each of the 10 generated datasets with known ground truth of $\Delta\alpha$. We used the same fitting procedures and priors as described in the main text. Using the fit models, we first tested whether the RL-ARD2 accurately recovered $\Delta\alpha$, which it did (Figure S5A). Next, we tested for which values of $\Delta\alpha$ our model comparison metric BPIC favors the RL-ARD2. Figure S5B demonstrates that the BPIC-differences start favoring the RL-ARD2 from a $\Delta\alpha \approx 0.05$ and higher.

We are not aware of earlier studies on SAT effects on learning rates, so direct comparison with the literature on this effect is not possible. However, between-trial differences in learning rates are studied in the context of asymmetries between learning rates for positive and negative reward prediction errors. For example, this asymmetry has been reported to vary between healthy controls and DYT1 dystonia patients, with a between-group difference of approximately 0.29 (19). In non-clinical contexts, it has been shown to differ as a function of ageing, with a mean difference of 0.22 (20). Our analysis here demonstrates that these effect sizes can be adequately detected by our methods and trial numbers.

Whole-brain GLMs.

Contrast 1: Speed-accuracy trade-off. First, we tested for regions that showed differential BOLD responses in the ‘SPD’ and ‘ACC’ conditions. In line with (21), we found that the anterior parts of the dorsal striatum and preSMA showed larger BOLD responses to ‘SPD’ compared to ‘ACC’ cues. With the increased spatial resolution and minimal smoothing applied in the current study, we spatially located the BOLD responses specifically in the posterior part of the head of the caudate, as well as the anterior part of the putamen (see Figure S1 for more detail on the clusters in subcortex). In addition, we found BOLD clusters in the thalamus. Based on the atlas of thalamic subnuclei from (22), the thalamic clusters corresponded to the ventral lateral (VL) nucleus, (38.3% of the cluster size in the left hemisphere, and 27.4% in the right hemisphere) and the ventral posterolateral (VPL) nucleus (15.2% and 8.2% for the left and right hemisphere, respectively). Furthermore, 9-13% of the cluster size corresponded to the CM nucleus, and 16-18% to the MD nucleus.

Contrast 2: Value and difficulty. The second contrast was the value difference contrast. This contrast tests for regions in which the size of the BOLD responses parametrically covary with the size of the *difference* in expected value between the two choice options, as estimated using the cognitive model. Due to the nature of this task, however, the contrast of value differences

112 conflates multiple cognitive factors (see also 23): The value difference determines the difficulty of the choice (higher value
113 differences imply easier decisions), and thereby influences the evidence accumulation process (drift rates), and related, the
114 (un)certainly regarding choices and the error rates. In part, the existing literature on perceptual decision making can help
115 interpretation, as difficulty effects for cortical areas are well-documented (for a meta-analysis, see 24) and include the (anterior)
116 insula, inferior frontal gyri, preSMA, and parietal regions that are more generally implicated in evidence accumulation such as
117 the lateral intraparietal sulcus. Indeed, this network of regions is found in the value difference contrast.

118 Additionally, we found BOLD responses in various parts of the striatum: The putamen showed a positive correlation between
119 value differences and BOLD responses, while the head of the caudate shows *negative* correlations.

120 **Contrast 3: Reward prediction errors.** The final contrast tested for regions showing a BOLD response of which the size covaried with
121 the size of the RPEs, as estimated by the RL-ARD model. In line with the literature (for early studies, see e.g. 25–27), we found
122 a clear BOLD cluster in ventral striatum (see Figure S1). The significant BOLD clusters covered many other regions across the
123 entire brain, including the occipital lobe. BOLD responses that covary with RPEs in the occipital lobe have been found before
124 in studies with comparable task paradigms (e.g., 28–30, see also the corresponding statistical parametric maps on neurovault:
125 collections at <https://identifiers.org/neurovault.collection:2007>, [neurovault.collection:2195](https://identifiers.org/neurovault.collection:2195), and [neurovault.collection:2222](https://identifiers.org/neurovault.collection:2222),
126 respectively). Furthermore, we found BOLD clusters in the ventral orbitofrontal cortex, another region often associated with
127 value processing (31). Subcortically, we found clusters in the putamen, amygdala, and hippocampus.

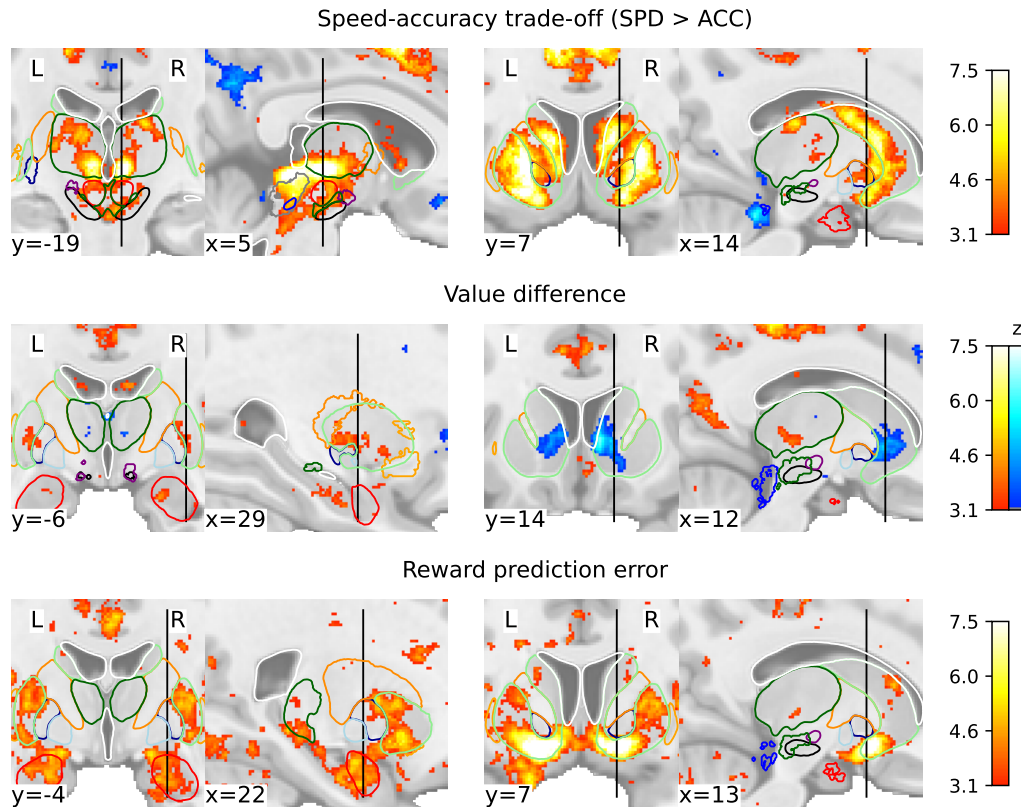


Fig. S1. Subcortical statistical parametric maps. Top row focuses on the thalamic (left) and striatal (right) clusters in the speed > accuracy contrast. Middle row focuses on the striatal clusters in the value difference contrast. Bottom row focuses on the amygdalar (left) and ventral striatal (right) clusters in the reward prediction error contrast. Coordinates are in MNI152NLin2009cAsym (1 mm) space. Thresholds were determined using the FDR method ($q < 0.05$), with a minimum of $z = 3.1$ to prevent overly liberal thresholds. Contours illustrate the following regions: Amg (red), Cl (orange), fx (light gray), GPe (dark blue), GPi (light blue), ic (dark orange), PAG (grey), PPN (blue), RN (red), SN (black), STN (purple), Str (light green), Tha (dark green), lateral, 3rd and 4th ventricles (white), and VTA (dark green). Masks in MNI152NLin2009cAsym space were obtained by first applying the MASSP algorithm to each participant between age 18–40 of the data of (32). The resulting voxelwise probabilistic masks in subject space were then non-linearly warped to MNI space, after which the across-subject best label was determined per voxel. Contours delineate best labels.

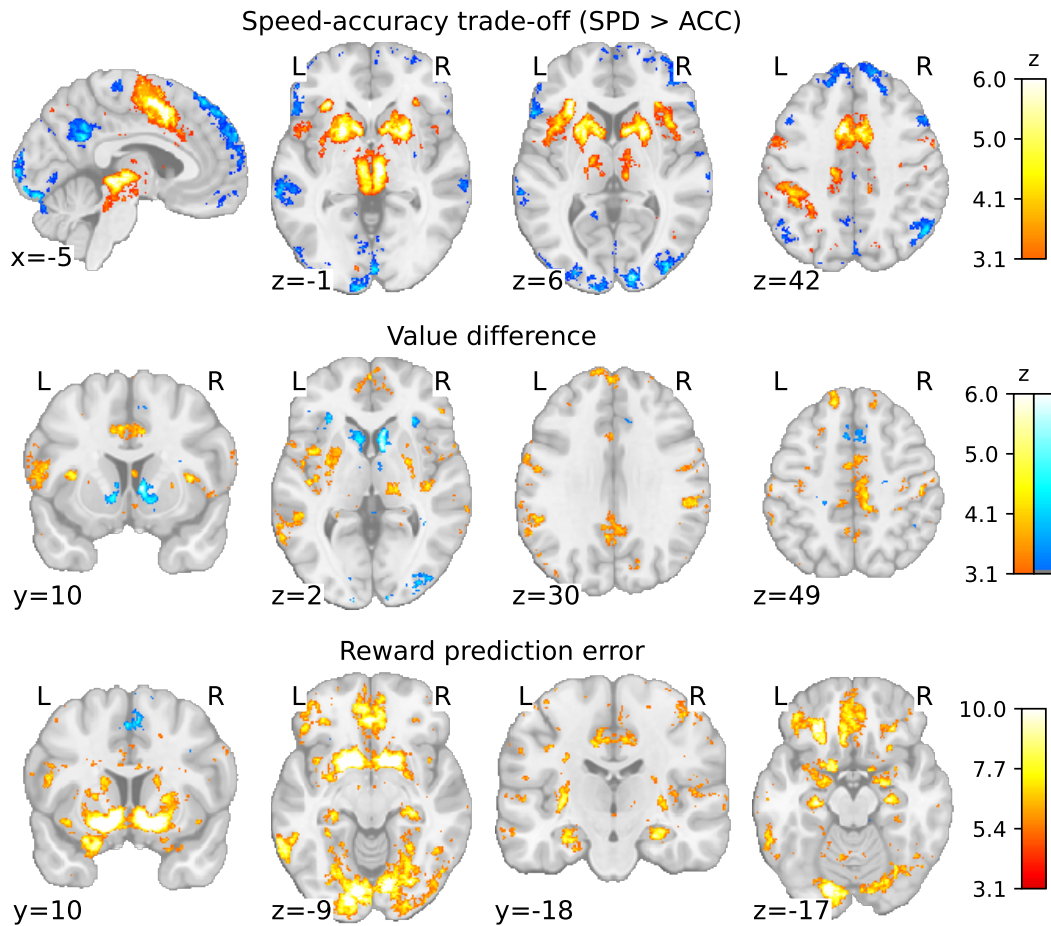


Fig. S2. Results of the voxelwise whole-brain GLMs. The three rows show the three main contrasts of interest: The speed-accuracy trade-off (top), value differences (middle), and reward prediction errors (bottom).

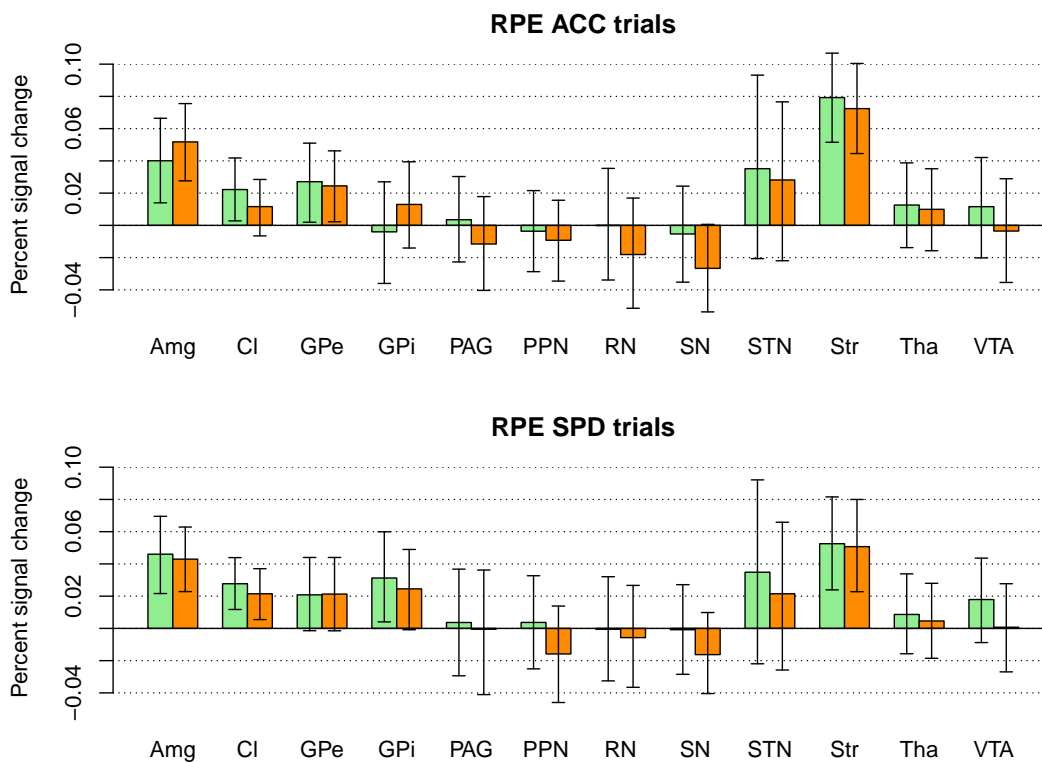


Fig. S3. Group-level estimates of within-participant brain-behavior relations of reward prediction errors in ACC (top) and SPD (bottom) trials. Barplots show the percentage signal change per unit change in reward prediction errors, for each region of interest. Green and orange bars depict the left and right hemisphere, respectively. Error bars indicate 95% credible intervals. Abbreviations refer to the amygdala (Amg), claustrum (Cl), globus pallidus interna (GPi) and externa (GPe), periaqueductal gray (PAG), pedunculopontine nucleus (PPN), red nucleus (RN) substantia nigra (SN), subthalamic nucleus (STN), striatum (Str), thalamus (Tha), and ventral tegmental area (VTA)

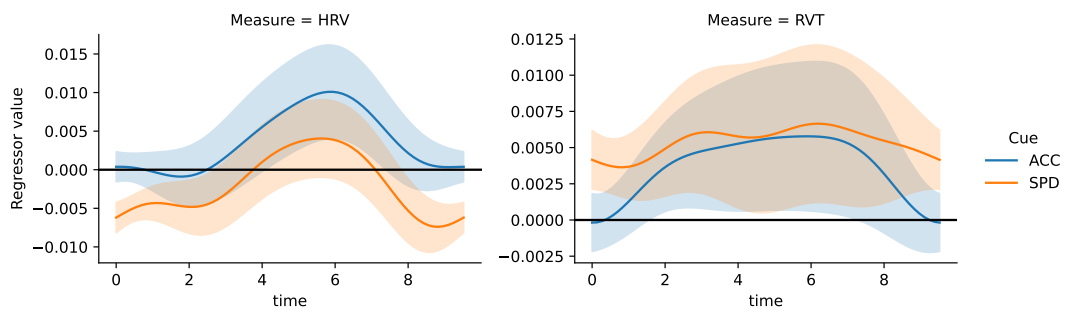


Fig. S4. Deconvolution of heart rate variability (HRV) and respiratory volume per time (RVT) responses to the cues using Fourier basis sets. Shaded areas correspond to 1 standard error.

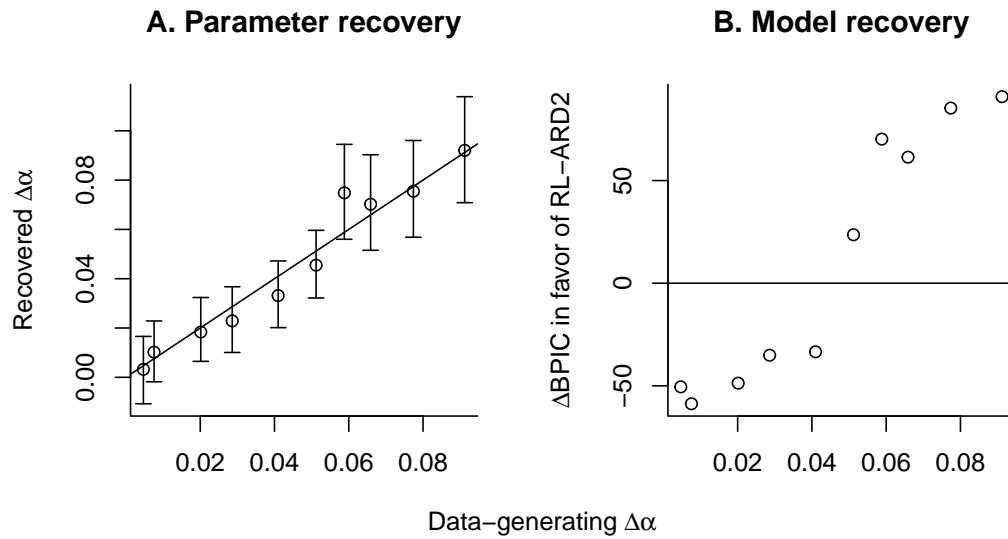


Fig. S5. A: Parameter recovery of the RL-ARD2 model for the $\Delta\alpha$ parameter. Values on the x-axis indicate data-generating parameters, and on the y-axis the median (points) and 95% credible interval (error bars) of the posteriors. B: Model recovery of the RL-ARD2 model. Values on the x-axis indicate data-generating parameters, and on the y-axis the BPIC difference between the RL-ARD2 and RL-ARD1. Larger values indicate a preference for the RL-ARD2; a difference of 0 (horizontal line) indicates no preference for either model.

Table S1. Correlation coefficients of parameters related to the speed-accuracy trade-off manipulation. Regions are from the MASSP delineations. Upper triangle displays means, lower triangle credible intervals. Abbreviations refer to the amygdala (Amg), claustrum (Cl), globus pallidus interna (GPi) and externa (GPe), periaqueductal gray (PAG), pedunculopontine nucleus (PPN), red nucleus (RN) substantia nigra (SN), subthalamic nucleus (STN), striatum (Str), thalamus (Tha), and ventral tegmental area (VTA) for the left (.l) and right (.r) hemisphere.

	u	B	Amg.l	Amg.r	Cl.l	Cl.r	GPe.l	GPe.r	GPi.l	GPi.r	PAG.l	PAG.r	PPN.l	PPN.r	RN.l	RN.r	SN.l	SN.r	STN.l	STN.r	Str.l	Str.r	Tha.l	Tha.r	VTA.l	VTA.r
u	1																									
B	.01-.63	1																								
Amg.l	-.41-.33	-.28-.45	1																							
Amg.r	-.38-.35	-.22-.47	-.2-.53	1																						
Cl.l	0-.65	-.23-.45	-.35-.4	-.19-.51	1																					
Cl.r	-.01-.65	-.26-.45	-.38-.36	-.21-.5	.35-.81	1																				
GPe.l	-.17-.53	-.34-.37	-.47-.29	-.22-.5	.21-.76	.19-.76	1																			
GPe.r	-.01-.65	-.24-.46	-.39-.36	-.27-.44	.35-.82	.32-.81	.21-.77	1																		
GPi.l	-.48-.24	-.46-.25	-.4-.36	-.16-.55	-.17-.54	-.22-.52	-.06-.62	-.29-.45	1																	
GPi.r	-.13-.6	-.23-.5	-.39-.38	-.21-.52	-.12-.74	.07-.7	-.08-.65	-.07-.71	-.24-.53	1																
PAG.l	-.32-.42	-.35-.36	-.34-.4	-.3-.43	-.26-.48	-.21-.52	-.25-.5	-.2-.55	-.34-.42	-.3-.46	1															
PAG.r	-.4-.4	-.4-.33	-.36-.4	-.35-.41	-.35-.46	-.34-.47	-.32-.46	-.34-.48	-.32-.48	-.35-.44	-.06-.62	1														
PPN.l	-.02-.63	-.14-.53	-.38-.39	-.31-.41	-.02-.63	.04-.68	-.09-.61	-.14-.73	-.46-.28	-.15-.58	-.05-.64	-.22-.56	1													
PPN.r	-.05-.63	-.22-.47	-.43-.35	-.34-.39	-.17-.75	.16-.74	-.02-.65	.27-.8	-.39-.35	-.04-.67	-.1-.61	-.24-.57	.23-.77	1												
RN.l	-.04-.65	-.25-.47	-.39-.4	-.42-.35	.03-.71	.04-.72	-.14-.63	.12-.75	-.48-.3	-.13-.63	-.23-.53	-.33-.5	.05-.71	.11-.75	1											
RN.r	-.02-.66	-.26-.44	-.42-.37	-.45-.28	-.02-.65	.01-.67	-.19-.53	.06-.69	-.54-.17	-.18-.57	-.23-.52	-.32-.51	.08-.71	.09-.72	.12-.73	1										
SN.l	-.11-.57	-.21-.48	-.41-.36	-.36-.37	-.03-.63	0-.66	-.16-.56	-.1-.71	-.44-.3	-.13-.59	-.11-.54	-.24-.54	.15-.73	.2-.76	.08-.72	.05-.68	1									
SN.r	-.01-.65	-.26-.43	-.49-.27	-.42-.32	.04-.69	.1-.72	.01-.68	.23-.77	-.44-.3	-.13-.62	-.11-.61	-.27-.54	.23-.76	.27-.79	.13-.75	.15-.74	.19-.75	1								
STN.l	-.3-.46	-.43-.31	-.33-.4	-.22-.49	.04-.67	.06-.69	.08-.71	.04-.69	-.16-.56	-.15-.58	-.23-.44	-.33-.44	-.12-.6	-.1-.6	-.18-.57	-.22-.51	-.23-.51	-.12-.6	1							
STN.r	-.12-.59	-.34-.38	-.38-.38	-.27-.46	.24-.78	.22-.77	.07-.72	.28-.8	-.26-.49	.03-.68	-.13-.6	-.25-.54	.1-.71	.2-.77	.06-.72	.03-.68	.09-.7	.14-.74	.02-.67	1						
Str.l	.08-.69	-.22-.46	-.44-.3	-.21-.48	.43-.84	.32-.81	.27-.78	.38-.82	-.18-.53	-.12-.75	-.19-.53	-.29-.52	.05-.67	.23-.77	.06-.73	-.03-.63	.06-.68	.18-.75	-.02-.64	.22-.77	1					
Str.r	-.09-.7	-.21-.47	-.45-.28	-.22-.49	.42-.83	.34-.81	.26-.78	.39-.83	-.18-.52	-.12-.74	-.16-.55	-.26-.54	.09-.69	.26-.78	.07-.74	-.01-.65	.09-.69	.22-.76	-.02-.64	.26-.78	.6-.89	1				
Tha.l	-.03-.63	-.26-.43	-.41-.34	-.18-.52	.39-.84	.32-.81	.38-.84	.4-.84	-.13-.57	-.06-.71	-.19-.54	-.27-.52	.07-.69	.2-.76	.02-.72	-.06-.63	.01-.66	.14-.74	.09-.71	.24-.79	.49-.86	.49-.86	1			
Tha.r	.06-.68	-.18-.49	-.37-.38	-.25-.47	.41-.84	.37-.83	.26-.79	.48-.86	-.28-.45	.07-.72	-.19-.55	-.31-.52	.21-.76	.33-.81	.18-.78	.11-.72	.15-.73	.26-.78	.06-.7	.3-.81	.48-.85	.48-.86	.5-.87	1		
VTA.l	.03-.66	-.18-.5	-.39-.37	-.32-.41	.19-.74	.24-.78	.04-.69	.35-.82	-.43-.31	-.01-.66	-.15-.59	-.29-.52	.3-.8	.35-.82	.19-.78	.19-.75	.25-.77	.33-.81	-.07-.65	.23-.78	.26-.77	.28-.78	.25-.78	.43-.84	1	
VTA.r	.1-.71	-.2-.49	-.41-.35	-.37-.36	.2-.76	.24-.79	.03-.68	.35-.82	-.46-.28	-.02-.68	-.17-.57	-.33-.52	.26-.78	.33-.81	.22-.8	.24-.77	.2-.76	.35-.81	-.06-.64	.23-.78	.26-.78	.28-.79	.24-.78	.43-.84	.46-.85	1

Table S2. Correlation coefficients of parameters related to the speed-accuracy trade-off manipulation. Regions are from the thalamic nuclei delineations. Upper triangle displays means, lower triangle credible intervals. Abbreviations refer to the anteroventral (AV), centromedian (CM), lateral posterior (LP), mediodorsal (MD), pulvinar, ventral anterior (VA), ventral lateral (VL), and the ventral posterolateral (VPL) nucleus. The MD is split into a lateral and medial part (MDl, MDm), the pulvinar in an anterior, inferior, lateral, and medial part (PuA, PuI, PuL, PuM), and the VL in an anterior and posterior part (VL.a, VL.p). Left and right hemisphere are indicated by .l and .r, respectively.

	u	B	AV.l	AV.r	CM.l	CM.r	LP.l	LP.r	MDl.l	MDl.r	MDm.l	MDm.r	PuA.l	PuA.r	PuI.l	PuI.r	PuL.l	PuL.r	PuM.l	PuM.r	VA.l	VA.r	VL.a.l	VL.a.r	VL.p.l	VL.p.r	VPL.l	VPL.r
u	1	.38	.39	.38	.37	.39	.17	.39	.3	.38	.41	.39	.41	.3	.19	.31	.32	.39	.42	.21	.31	.23	.4	.3	.4	.37	.35	
B	.06-.64	1	.24	.11	.15	.13	.03	.17	.11	.17	.15	.17	.17	.15	.06	.12	.14	.15	.19	.03	.03	.03	.14	.09	.18	.19	.19	
AV.l	.03-.68	-.11-.55	1	.65	.59	.59	.56	.55	.64	.68	.68	.69	.68	.66	.62	.51	.64	.6	.68	.67	.56	.56	.61	.65	.66	.69	.68	.64
AV.r	.02-.67	-.24-.46	.39-.84	1	.61	.6	.6	.59	.66	.73	.69	.73	.71	.73	.64	.57	.67	.67	.7	.71	.58	.66	.63	.74	.68	.74	.68	.68
CM.l	.02-.66	-.21-.49	.29-.8	.31-.82	1	.6	.53	.53	.62	.69	.66	.69	.66	.64	.62	.52	.61	.62	.67	.66	.54	.59	.59	.66	.64	.68	.65	.65
CM.r	.03-.68	-.24-.47	.28-.81	.31-.81	.31-.81	1	.53	.55	.6	.68	.64	.67	.64	.66	.59	.51	.64	.6	.66	.66	.55	.54	.58	.63	.61	.68	.63	.62
LP.l	-.24-.53	-.32-.4	.25-.79	.3-.81	.19-.78	.19-.78	1	.5	.65	.67	.66	.67	.64	.64	.58	.54	.67	.64	.64	.63	.6	.61	.66	.62	.68	.67	.63	.62
LP.r	.03-.69	-.19-.51	.24-.78	.3-.8	2-.77	.23-.78	.14-.76	1	.53	.63	.57	.62	.61	.65	.55	.53	.61	.6	.6	.65	.47	.55	.53	.63	.58	.66	.62	.63
MDl.l	-.08-.63	-.26-.46	.37-.83	.4-.85	.32-.82	.29-.81	.37-.84	.19-.78	1	.73	.76	.75	.74	.69	.66	.54	.69	.67	.73	.68	.66	.65	.71	.69	.75	.72	.71	.65
MDl.r	.01-.67	-.18-.51	.43-.85	.51-.88	.42-.86	.41-.86	.38-.85	.35-.83	.49-.88	1	.76	.82	.78	.8	.71	.63	.76	.76	.78	.8	.64	.71	.8	.75	.83	.76	.77	
MDm.l	.02-.67	-.2-.49	.44-.85	.44-.86	.38-.85	.36-.84	.39-.85	.25-.8	.56-.9	.55-.9	1	.8	.77	.73	.68	.55	.72	.7	.78	.72	.67	.68	.71	.73	.76	.75	.72	.68
MDm.r	.06-.7	-.19-.49	.44-.85	.5-.88	.42-.86	.4-.86	.39-.85	.33-.83	.53-.89	.65-.92	.61-.91	1	.78	.79	.7	.6	.75	.74	.8	.79	.66	.72	.71	.79	.76	.81	.74	.74
PuA.l	.03-.69	-.19-.51	.43-.85	.47-.87	.38-.85	.36-.84	.35-.84	.31-.82	.51-.88	.57-.9	.56-.9	.59-.91	1	.75	.69	.6	.73	.71	.78	.76	.63	.68	.71	.76	.76	.78	.76	.72
PuA.r	.06-.7	-.18-.5	.39-.84	.5-.87	.36-.84	.39-.85	.35-.84	.37-.84	.43-.86	.63-.91	.5-.88	.6-.91	.53-.89	1	.67	.63	.76	.74	.75	.79	.62	.69	.69	.78	.72	.81	.74	.76
PuI.l	-.08-.62	-.21-.49	.33-.82	.35-.84	.33-.83	.28-.81	.24-.81	.21-.79	.37-.85	.46-.87	.4-.86	.43-.87	.43-.87	.39-.85	1	.57	.64	.65	.68	.67	.57	.61	.63	.69	.69	.71	.69	.66
PuI.r	-.21-.55	-.31-.42	.16-.76	.25-.8	.18-.77	.17-.77	.19-.8	.18-.78	.19-.79	.33-.84	.2-.79	.29-.82	.28-.82	.31-.83	.24-.8	1	.62	.6	.59	.63	.49	.55	.59	.62	.61	.66	.62	.65
PuL.l	-.06-.63	-.24-.46	.37-.83	.41-.85	.3-.82	.37-.84	.4-.86	.32-.83	.45-.86	.56-.89	.5-.87	.55-.89	.5-.88	.56-.89	.35-.83	.3-.83	1	.74	.74	.76	.64	.65	.72	.72	.75	.78	.75	.73
PuL.r	-.06-.63	-.21-.47	.31-.81	.42-.85	.33-.82	.32-.82	.36-.84	.3-.82	.4-.85	.54-.89	.46-.86	.51-.88	.46-.87	.53-.89	.37-.84	.29-.82	.51-.88	1	.71	.73	.59	.66	.67	.73	.72	.77	.72	.73
PuM.l	.03-.68	-.2-.49	.44-.85	.46-.87	.4-.85	.38-.85	.36-.84	.29-.82	.5-.88	.58-.91	.57-.9	.6-.91	.57-.9	.53-.89	.42-.86	.26-.82	.52-.89	.46-.87	1	.76	.64	.68	.71	.76	.75	.78	.75	.72
PuM.r	.07-.7	-.17-.53	.42-.85	.47-.86	.39-.84	.4-.85	.33-.83	.37-.84	.43-.86	.62-.91	.49-.88	.6-.9	.55-.89	.6-.9	.4-.85	.34-.84	.55-.89	.5-.88	.55-.89	1	.59	.67	.69	.77	.73	.8	.76	.77
VA.l	-.17-.33	-.33-.57	.25-.8	.27-.81	.21-.78	.24-.8	.29-.82	.11-.74	.37-.85	.35-.84	.4-.86	.38-.85	.32-.83	.32-.83	.24-.81	.13-.77	.34-.84	.26-.81	.34-.84	.27-.81	1	.6	.64	.61	.65	.64	.59	.56
VA.r	-.07-.33	-.33-.38	.26-.79	.4-.84	.29-.8	.23-.78	.31-.83	.23-.79	.38-.84	.46-.87	.42-.86	.48-.88	.42-.86	.45-.86	.31-.82	.22-.79	.37-.84	.39-.85	.41-.86	.41-.85	.29-.82	1	.64	.72	.67	.7	.63	.63
VL.a.l	-.14-.58	-.32-.39	.33-.81	.35-.83	.27-.8	.28-.81	.39-.85	.2-.78	.49-.87	.48-.87	.48-.87	.48-.87	.47-.87	.43-.86	.34-.83	.27-.82	.49-.88	.41-.85	.49-.87	.44-.87	.35-.84	.34-.83	1	.68	.75	.73	.72	.68
VL.a.r	.05-.69	-.22-.48	.38-.84	.52-.88	.39-.84	.33-.83	.31-.83	.34-.83	.44-.87	.62-.91	.5-.88	.6-.91	.55-.9	.59-.9	.42-.87	.32-.83	.48-.87	.5-.88	.54-.9	.57-.89	.29-.83	.49-.88	.41-.85	1	.73	.81	.73	.75
VL.p.l	-.08-.62	-.26-.44	.4-.84	.43-.85	.36-.84	.31-.82	.41-.86	.26-.81	.54-.89	.54-.89	.55-.89	.54-.89	.54-.89	.49-.87	.42-.86	.28-.83	.53-.88	.48-.87	.54-.89	.5-.88	.37-.85	.39-.85	.54-.89	.48-.88	1	.77	.77	.72
VL.p.r	.04-.69	-.17-.51	.44-.86	.53-.88	.42-.85	.42-.86	.4-.85	.39-.85	.49-.88	.67-.92	.54-.89	.63-.91	.58-.9	.64-.92	.45-.87	.36-.85	.58-.9	.57-.9	.58-.9	.63-.91	.35-.84	.45-.86	.5-.88	.63-.91	.56-.89	1	.78	.79
VPL.l	0-.67	-.16-.52	.42-.85	.42-.85	.37-.84	.34-.83	.32-.84	.32-.82	.46-.87	.55-.9	.5-.87	.53-.89	.55-.89	.52-.89	.44-.86	.31-.83	.53-.89	.48-.87	.53-.89	.55-.89	.27-.82	.34-.83	.48-.87	.5-.88	.56-.9	.59-.91	1	.76
VPL.r	-.02-.65	-.16-.52	.37-.83	.43-.85	.38-.84	.33-.82	.31-.83	.34-.83	.38-.84	.57-.9	.42-.85	.51-.88	.5-.87	.56-.89	.39-.85	.35-.84	.51-.88	.49-.88	.47-.88	.57-.9	.23-.79	.35-.83	.42-.85	.53-.88	.49-.88	.61-.91	.54-.89	1

Table S4. Participant-wise BPIC values of the single and two-learning rate RL-ARDs.

	Single learning rate	Two learning rates
1	-11.98	-12.67
2	-327.31	-316.69
3	325.19	328.75
4	-185.30	-185.07
5	-180.31	-180.32
6	13.88	15.21
7	-84.10	-82.15
8	362.84	360.08
9	-618.58	-610.70
10	236.33	234.82
11	-95.55	-89.54
12	121.78	124.49
13	252.66	253.01
14	9.60	16.15
15	-3.81	0.55
16	-4.23	-2.38
17	454.04	450.42
18	-50.88	-50.92
19	23.05	25.64
20	-83.99	-83.62
21	-93.46	-92.04
22	-136.47	-135.78
23	-117.94	-117.23
24	444.98	450.99
25	-52.22	-53.51
26	-81.39	-80.05
27	-105.28	-104.20
28	200.37	200.48
29	-77.28	-75.16
30	102.42	107.69
31	170.76	169.07
32	12.72	16.76
33	151.16	151.61
34	-98.24	-99.05
35	-39.18	-36.30
36	326.13	328.99
37	-197.81	-198.17

References

1. NJ Tustison, et al., N4ITK: Improved N3 Bias Correction. *IEEE Transactions on Med. Imaging* **29**, 1310–1320 (2010).
2. B Avants, C Epstein, M Grossman, J Gee, Symmetric diffeomorphic image registration with cross-correlation: Evaluating automated labeling of elderly and neurodegenerative brain. *Med. Image Analysis* **12**, 26–41 (2008).
3. Y Zhang, M Brady, S Smith, Segmentation of brain MR images through a hidden Markov random field model and the expectation-maximization algorithm. *IEEE Transactions on Med. Imaging* **20**, 45–57 (2001).
4. M Reuter, HD Rosas, B Fischl, Highly accurate inverse consistent registration: A robust approach. *NeuroImage* **53**, 1181–1196 (2010).
5. AM Dale, B Fischl, MI Sereno, Cortical Surface-Based Analysis. *NeuroImage* **9**, 179–194 (1999).
6. A Klein, et al., Mindboggling morphometry of human brains. *PLOS Comput. Biol.* **13**, e1005350 (2017).
7. V Fonov, A Evans, R McKinstry, C Almlil, D Collins, Unbiased nonlinear average age-appropriate brain templates from birth to adulthood. *NeuroImage* **47**, S102 (2009).
8. RW Cox, JS Hyde, Software tools for analysis and visualization of fMRI data. *NMR Biomed.* **10**, 171–178 (1997).
9. DN Greve, B Fischl, Accurate and robust brain image alignment using boundary-based registration. *NeuroImage* **48**, 63–72 (2009).
10. M Jenkinson, P Bannister, M Brady, S Smith, Improved Optimization for the Robust and Accurate Linear Registration and Motion Correction of Brain Images. *NeuroImage* **17**, 825–841 (2002).
11. JD Power, et al., Methods to detect, characterize, and remove motion artifact in resting state fMRI. *NeuroImage* **84**, 320–341 (2014).
12. Y Behzadi, K Restom, J Liu, TT Liu, A component based noise correction method (CompCor) for BOLD and perfusion based fMRI. *NeuroImage* **37**, 90–101 (2007).

- 149 13. TD Satterthwaite, et al., An improved framework for confound regression and filtering for control of motion artifact in the
150 preprocessing of resting-state functional connectivity data. *NeuroImage* **64**, 240–256 (2013).
- 151 14. C Lanczos, Evaluation of Noisy Data. *J. Soc. for Ind. Appl. Math. Ser. B Numer. Analysis* **1**, 76–85 (1964).
- 152 15. A Abraham, et al., Machine learning for neuroimaging with scikit-learn. *Front. neuroinformatics* **8**, 14 (2014).
- 153 16. E Bullmore, et al., Statistical methods of estimation and inference for functional MR image analysis. *Magn. Reson.*
154 *Medicine* **35**, 261–277 (1996).
- 155 17. DR Gitelman, WD Penny, J Ashburner, KJ Friston, Modeling regional and psychophysiologic interactions in fMRI: The
156 importance of hemodynamic deconvolution. *NeuroImage* **19**, 200–207 (2003).
- 157 18. G De Hollander, T Knapen, L Snoek, Nideconv (2019).
- 158 19. D Arkadir, et al., DYT1 dystonia increases risk taking in humans. *eLife* **5**, e14155 (2016).
- 159 20. GM Rosenbaum, HL Grassie, CA Hartley, Valence biases in reinforcement learning shift across adolescence and modulate
160 subsequent memory. *eLife* **11**, e64620 (2022).
- 161 21. BU Forstmann, et al., Striatum and pre-SMA facilitate decision-making under time pressure. *Proc. Natl. Acad. Sci. United*
162 *States Am.* **105**, 17538–17542 (2008).
- 163 22. JE Iglesias, et al., A probabilistic atlas of the human thalamic nuclei combining ex vivo MRI and histology. *NeuroImage*
164 **183**, 314–326 (2018).
- 165 23. JP O’Doherty, The problem with value. *Neurosci. Biobehav. Rev.* **43**, 259–268 (2014).
- 166 24. MC Keuken, et al., Brain networks of perceptual decision-making: an fMRI ALE meta-analysis. *Front. Hum. Neurosci.* **8**
167 (2014).
- 168 25. SM McClure, GS Berns, PR Montague, Temporal prediction errors in a passive learning task activate human striatum.
169 *Neuron* **38**, 339–346 (2003).
- 170 26. JP O’Doherty, et al., Dissociable Roles of Ventral and Dorsal Striatum in Instrumental Conditioning. *Science* **304**, 452–454
171 (2004).
- 172 27. JP O’Doherty, P Dayan, KJ Friston, HD Critchley, RJ Dolan, Temporal Difference Models and Reward-Related Learning
173 in the Human Brain. *Neuron* **28**, 329–337 (2003).
- 174 28. TU Hauser, E Eldar, RJ Dolan, Separate mesocortical and mesolimbic pathways encode effort and reward learning signals.
175 *Proc. Natl. Acad. Sci. United States Am.* **114**, E7395–E7404 (2017).
- 176 29. G Lefebvre, M Lebreton, F Meyniel, S Bourgeois-Gironde, S Palminteri, Behavioural and neural characterization of
177 optimistic reinforcement learning. *Nat. Hum. Behav.* **1**, 1–9 (2017).
- 178 30. GE Wimmer, ND Daw, D Shohamy, Generalization of value in reinforcement learning by humans. *Eur. J. Neurosci.* **35**,
179 1092–1104 (2012).
- 180 31. ML Kringelbach, ET Rolls, The functional neuroanatomy of the human orbitofrontal cortex: Evidence from neuroimaging
181 and neuropsychology. *Prog. Neurobiol.* **72**, 341–372 (2004).
- 182 32. S Miletić, et al., Charting human subcortical maturation across the adult lifespan with in vivo 7 T MRI. *NeuroImage* **249**,
183 118872 (2022).